Hearing Research 393 (2020) 108013

Contents lists available at ScienceDirect

Hearing Research

journal homepage: www.elsevier.com/locate/heares

Research Paper

Expression patterns of chloride transporters in the auditory brainstem of developing chicken

Marcus J. Wirth [a, *], Tobias Ackels [b, c, 1], Andreas Kriebel [d, 1], Katharina Kriebel [d, 1], Jörg Mey [a, e], Thomas Kuenzel [a], Hermann Wagner [d]

[a] Department for Chemosensation, RWTH Aachen University, Aachen, Germany
[b] Neurophysiology of Behaviour Lab, The Francis Crick Institute, London, United Kingdom
[c] Department of Neuroscience, Physiology and Pharmacology, University College London, London, United Kingdom
[d] Department for Zoology and Animal Physiology, RWTH Aachen University, Aachen, Germany
[e] Hospital Nacional de Parapléjicos, Toledo, Spain

ARTICLE INFO

Article history:
Received 5 September 2019
Received in revised form
29 April 2020
Accepted 29 May 2020
Available online 3 June 2020

Keywords:
Chloride homeostasis
Nucleus laminaris
Nucleus magnocellularis
GABA
KCC2
NKCC1

ABSTRACT

GABAergic transmission changes from depolarization to hyperpolarization in most vertebrate brain regions during development. By contrast, in the auditory brainstem of chicken a depolarizing effect of GABA persists after hatching. Since auditory brainstem neurons that receive GABAergic input have a Cl^- reversal potential above resting membrane potential, a specifically tuned activity of Cl^- transporters is likely. We here present a developmental study of the expression patterns of several members of the SLC12 family (NKCC1, NKCC2, KCC1, KCC2, KCC4, CCC6, CCC9) and of AE3 at developmental ages E7, E10, E12, E15, E17, and P1 with quantitative RT-PCR. NKCC2 and CCC9 were not detected in auditory brainstem (positive control: kidney). KCC1, CCC6 and AE3 were expressed, but not regulated, while NKCC1, KCC2 and KCC4 were regulated. The expression of the latter transporters increased, with KCC2 exhibiting the strongest expression at all time points. Biochemical analysis of the protein expression of NKCC1, KCC2 and KCC4 corroborated the findings on the mRNA level. All three transporters showed a localization at the outer rim of the cells, with NKCC1 and KCC2 expressed in neurons, and KCC4 predominantly in glia. The comparison of the published chloride reversal potential and expression of transporter proteins suggest strong differences in the efficiency of the three transporters. Further, the strong KCC2 expression could reflect a role in the structural development of auditory brainstem synapses that might lead to changes in the physiological properties.

1. Introduction

Chloride serves multiple roles in neuronal signaling. Different cell types can have vastly different cytosolic chloride concentrations (for review see Friauf et al., 2011). The chloride equilibrium potential (E_{Cl}) can be actively adjusted via chloride channels and active chloride transporters to levels above or below the resting membrane potential leading to outward or inward currents upon chloride channel opening via $GABA_A$ or glycine receptor channels.

In the chicken auditory brainstem, the GABA equilibrium potential is higher than the firing threshold, but the neurons do not fire upon opening of GABAergic channels due to the activation of low-voltage activated dendrotoxin-I-sensitive potassium channels (Monsivais and Rubel, 2001). The avian auditory brainstem is composed of Nucleus angularis (NA), Nucleus magnocellularis (NM; together with NA representing the avian cochlear nucleus) and Nucleus laminaris (NL, homologous to medial superior olive). They show a high amount of $GABA_A$ receptor-mediated inhibition (Kuo et al., 2009). $GABA_A$ receptors are present as early as embryonic day 13 and their expression appears to be higher in embryos than in hatched chicken (Code and Churchill, 1991). The significant physiological importance of GABAergic inhibition has been described extensively (Hyson et al., 1995; Funabiki et al., 1998; Yang et al., 1999; Monsivais et al., 2000; Monsivais and Rubel, 2001; Yamada et al., 2013; Ohmori, 2014). All three nuclei, NA, NM and NL, receive GABAergic inhibition from the superior olivary nucleus (SON) that is tonotopically organized (Tabor et al., 2012). A second

* Corresponding author. Institute of Biology II, Department of Chemosensation, Worringer Weg 3, D-52074, Aachen, Germany.
E-mail address: wirth@bio2.rwth-aachen.de (M.J. Wirth).
[1] These authors contributed equally.

https://doi.org/10.1016/j.heares.2020.108013
0378-5955/

source of GABAergic inhibition are local interneurons surrounding NL (Müller, 1987). In the auditory pathway, inhibition mediated by chloride ions plays a role in tuning the responses of cells to the sound-localization parameter interaural time difference (ITD). This happens via shunting inhibition at several stations, and most importantly in cells of the avian NM and NL (Monsivais et al., 2000) that will be investigated in this study.

The E_{Cl} depends on the intracellular chloride concentration which is tightly regulated by chloride transporters. Most chloride transporters in the brain studied so far belong to the family of cation-chloride cotransporters (CCC) which were first detected in cartilaginous and teleost fish (Gamba et al., 1993; Xu et al., 1994). The CCC family, also known as SLC12 family, comprises two main branches, the sodium-driven transporters and the potassium-driven transporters. The first branch contains inward-directed chloride transporters: the two bumetanide-sensitive Na^+-K^+-$2Cl^-$ -cotransporters NKCC1 (SLC12A2) and NKCC2 (SLC12A1), and the thiazide-sensitive Na^+-Cl^- -cotransporter NCC (SLC12A3). The latter two show a mostly renal expression (for review: Blaesse et al., 2006; Friauf et al., 2011). The second branch encompasses four members, which encode the outward-directed K^+-Cl^- - cotransporters KCC1 to KCC4 (SLC12A4-7) (Adragna et al., 2004). All four are expressed in neural cells with KCC2 being neuron-specific (Payne et al., 1996). KCC3, while present in fish, amphibians, reptiles and mammals, seems to be absent in birds (Gagnon and Delpire, 2013). The last two members of the family are CCC9 (SLC12A8), which is known to transport polyamines and amino acids (Daigle et al., 2009), and CCC6 (CIP1, SLC12A9), whose substrates and physiological role are still unclear. Another chloride-transporter family not belonging to the CCCs is the anion-exchanger (AE) family with its members AE1 to 3 which exchange HCO_3^- with Cl^-. AE3 (SLC4A3) is known to be expressed in neural cells (Kobayashi et al., 1994) and is described as an inward-directed transporter (Becker et al., 2003).

To shed more light on the molecular basis of the elevated E_{Cl} in auditory brainstem neurons in chicken we identified the transporters expressed in embryonic and hatchling stages and quantified mRNA and protein expression during development. Further, we quantified the developmental changes of the intracellular expression patterns of selected transporters in NM cells.

2. Materials and methods

2.1. Tissue preparation

All experiments were conducted according to German Federal law and Council Directive 2010/63EU of the European Parliament and the Council of 22 September 2010 on the protection of animals used for scientific purposes and were approved by local authorities. Fertilized eggs of White Leghorn Chicken (*Gallus gallus L.*) were received from a local chicken farm. The eggs were incubated at 37 °C at 50% humidity and a rotation cycle of 7.5 cycles per hour for 7, 9, 12, 15 and 18 days (E7 – E18) or until hatching (P1).

Embryos were harvested by fenestration of the egg and subsequent decapitation of the embryo. A staging according to Hamburger and Hamilton (1951) was performed (Table 1). Hatched chicken were deeply anaesthetized with isoflurane and perfused with ice-cold ringer solution. For immunohistochemistry, animals were perfused subsequently with 4% phosphate-buffered formalin solution.

The optic tectum and the auditory brainstem were prepared using fine scissors and forceps (Dupont no. 5). Meninges were removed and the brain parts were kept in ice-cold ringer solution. From some chicken, kidneys were harvested as control tissue.

Table 1
Staging of embryos according to Hamburger and Hamilton (1951).

Days of incubation	7	9	12	15	18
Hamburger-Hamilton-stages	29–33	34–36	37–39	40–42	43–45

2.2. PCR

For each age and tissue, samples of 20–50 mg were collected in 0.5 ml “Allprotect Tissue Reagent” (Quiagen, Germany) to prevent mRNA degradation. Extraction was performed with “RNeasy Lipid Tissue Mini Kit” (Quiagen, Germany) using an ultrasonic tissue homogenizer. Reverse transcription was performed with an “Omniscript RT Kit” (Quiagen, Germany). Primer against the transporter sequences and the standard gamma-actin (ACTG1) and glyceraldehyde 3-phosphate dehydrogenase (GAPDH) were designed using sequences from ENSEMBL genome database searches for the transporter in the *Gallus gallus* genome. Due to the lack of a chicken KCC2 sequence, a search in the genome of the zebrafinch (*Taeniopygia guttata*) and a homology search with BLAST in the chicken genome was performed. Primer sequences can be found in Table 2. All primers were ordered from Sigma-Aldrich (Germany). Functionality and specificity were tested with endpoint PCR on cDNAs derived from whole brain and kidney tissue. PCR was performed with the “Red TAQ ReadyMix PCR-reaction kit” (Sigma Aldrich, Germany) on an “ICycler” (Biorad, Germany). The PCR protocol included initial denaturation for 3 min at 94 °C, and 35 cycles of denaturation for 30 s at 94 °C, annealing for 45 s at 59 °C, elongation for 90 s at 72 °C and a final elongation at 72 °C for 10 min. The products were separated on a 1.5% agarose gel for analysis. The optimal annealing temperature was determined via temperature gradient PCR.

Quantitative real-time PCR was performed using the Biorad “ICycler” and the “MyIQ” detection system with the “Biorad IQ5 Optical System Software 2.0” (all Biorad, Germany) and “SYBRGreen PCR Master Mix” (Quiagen, Germany) and 5 ng cDNA per amplification. The PCR program included initial denaturation for 15 min at 94 °C, and 40 cycles of denaturation for 20 s at 94 °C, annealing for 20 s at 57 °C or 59 °C depending on the primer, elongation for 20 s at 72 °C and the fluorescent measurement for 15 s at 74 °C. The melting point was determined in the third cycle. The amplification rate for each transcript was calculated. For the analysis of the threshold cycles (ct) a threshold of 500 units was set manually. Threshold values of ACTG1 and GAPDH were determined five times for each developmental age. ACTG1 showed less deviation from the mean compared to GAPDH during the development and therefore was chosen as standard. The delta-ct was calculated via subtraction of the ct of the standard and the ct of the transporter transcript. Together with the amplification rate, the relative amount of mRNA was calculated. The mean and the standard error of four replications of each transcript and time point were calculated and presented as bar plots. Data were tested for normal distribution with a Kolmogorov-Smirnov-test. One-factor univariate analysis of variance (ANOVA) was performed to detect statistically significant differences. If such differences were detected pairwise post-hoc testing (Tukey-Kramer) was performed.

2.3. Biochemistry

Tissue samples were weighed and then dissolved in 2.5 times volume per weight phosphate buffer with 1% protease inhibitor cocktail (Sigma-Aldrich, Germany) employing an ultrasonic tissue homogenizer. The solution was spun down at 12,000 RPM at 4 °C and the supernatant was collected. Protein concentration was

Table 2
Primer sequences with identification number of the transcripts from the ENSEMBL database and the expected product size in base pairs (bp).

Gene	transcript ID	direction	sequence	Product size
NKCC1	ENSGALT00000023675	sense	AGGCTCCTGTGTTGTTCGAG	161 bp
	ENSGALT00000037717	antisense	TGCTCATCACCTGGAAATTG	
NKCC2	ENSGALT00000007915	sense	AAGGGCGTGCTGGTAAGAT	188 bp
		antisense	CCACCTCCACGGACAAAC	
KCC1	ENSGALT00000005597	sense	GAAAGGGAGGCTCAGCTAGTAA	203 bp
		antisense	GATTGGTTCGGTTTAATGCTG	
KCC2	ENSGALT00000011227	sense	TTTGCTGCTCCTGTACGATG	212 bp
		antisense	GAAGATGTAGGCCAGCAGGA	
KCC4	ENSGALT00000020422	sense	AGTCAAGGTTCCACGAATGG	161 bp
	ENSGALT00000037368	antisense	TGCAGTTAGCATAGTACAAGCACA	
CCC6	ENSGALT00000012821	sense	TTGGACACACTGCCCTCAG	195 bp
		antisense	ATCATCGTAGAAGCCCAGCA	
CCC9	ENSGALT00000019681	sense	CGTTCACCAGCAAAAATCCT	211 bp
		antisense	TCTCATGCCTCTGTAGCAGGT	
AE3	ENSGALT00000018302	sense	GTGGTCCTTGTGGGTTGC	213 bp
		antisense	AGCCTCATGGAAATGCTTGT	
ACTG1	ENSGALT00000039969	sense	GAGGGAGATCGTCCGTGATA	188 bp
	ENSGALT00000002103	antisense	CCAGGAAGGAAGGTTGGAAG	

determined with the "BCA-Kit" (Sigma-Aldrich, Germany). Proteins were separated by SDS-PAGE and transferred to a nitrocellulose membrane via tank blotting. The quality of the transfer and the loading equilibrium were analyzed with a Ponceau S staining. Unspecific binding sites on the membranes were blocked with "The Blocking Solution" (Candor Bioscience, Wangen, Germany) at 4 °C over-night. Primary antibodies were dissolved in "LowCross Buffer" (Candor Bioscience). All antibodies were polyclonal. For origin of species and dilution see Table 3. Detection of the primary antibodies was performed with peroxidase-coupled secondary antibodies (Table 3), enhanced chemiluminescence (GE Healthcare) and x-ray film. Exposure time varied between 1 and 40 min but was kept the same for each antigen. X-ray films were developed with Dokumol and Superfix Plus (Tetenal, Germany) with identical conditions for all antigens. After detection of the transporters, the blots were stripped and the same detection procedure was performed for actin. The protein bands on the x-ray films were captured photographically and analyzed densitometrically. Transporter expression was normalized to actin expression. Specificity of the antibodies was tested via pre-incubation with peptide homologues of the epitopes (Table 3) and analysis of kidney lysates as positive control for NKCC1 and KCC4 and negative control for KCC2 (Fig. 2).

The mean and the standard error of the mean of four replications of each protein and time point were calculated and presented as bar plots. Data were tested for normal distribution with a Kolmogorov-Smirnov-test. One-factor univariate analysis of variance (ANOVA) was performed to detect statistically significant differences and followed up by a Tukey-Kramer test.

2.4. Immunohistochemistry

Embryonic auditory brainstem (E12, E15, E18) was fixed by immersion for 24 h in 4% formalin solution. Brains of hatched animals (P1) were fixated by perfusion of the animal with 4% formalin solution. Cryoprotection was achieved with immersion in 15% and 30% sucrose. Tissue was stored at −80 °C until 30 μm slices were prepared by cutting on a Leica CM3050S cryostat microtome (Leica, Germany). Nissl staining with 1% cresyl violet was performed on sets of slices from all developmental ages and analyzed to identify

Table 3
Primary antibodies, peptides and dilutions.

Antigen	Species	Vendor Catl. #	Stock concentration	Dilution
NKCC1	Rabbit	Millipore, USA #AB3560P	1 mg/ml	1:500
NKCC1 peptide		Millipore, USA #on request	1 mg/ml	Used 10 times the antibody weight
KCC2	Rabbit	Abcam, United Kingdom #ab49917	1 mg/ml	1:1000
KCC2 peptide		Lifespan Biosciences, USA #LS-PC24942	1 mg/ml	Used 10 times the antibody weight
KCC4	Goat	Santa Cruz Biotechnology, USA #sc-19427	200 μg/ml	1:500
KCC4 peptide		Santa Cruz Biotechnology, USA #sc-19427 P	200 μg/ml	Used 10 times the antibody weight
actin	Rabbit	Sigma-Aldrich, Germany #SAB4301137	1 mg/ml	1:1000
Calretinin (in combination with NKCC1 and KCC2)	Goat	Millipore, USA #ab1550	1 mg/ml	1:500
Calretinin (in combination with KCC4)	Rabbit	Sigma, Germany #C7479	1 mg/ml	1:500
PLP	Mouse	Millipore, USA #MAB388	1 mg/ml	1:200
GFAP	Mouse	Millipore, USA #MAB360	1 mg/ml	1:500

the auditory nuclei NL and NM. Unspecific binding sites in the other slices were blocked with incubation for 60–90 min in 4% normal horse serum and 0.4% Triton-X-100 in 0.05 M Tris-buffered saline. Primary antibodies against NKCC1, KCC2 and KCC4 were the same as for the biochemical analysis. Concentrations were 5 μg/ml for rabbit-anti-NKCC1, 1 μg/ml for rabbit-anti-KCC2 and 5 μg/ml for goat-anti-KCC4. To identify auditory brainstem neurons two antibodies against calretinin were used for double-staining with the transporters. Goat-anti-calretinin (Millipore, Germany) was used together with anti-NKCC1 or anti-KCC2. Rabbit-anti-calretinin (Sigma, Germany) was used together with anti-KCC4. To detect co-localization of KCC4 with glia cells co-staining either against glial acidic fibrillary protein ((GFAP), mouse-anti-GFAP, 2 μg/ml, Millipore, Germany) or against myelin (mouse-anti-proteo-lipid-protein, 5 μg/ml, Millipore, Germany) were performed on subsequent slices. All secondary antibodies were raised in donkey, either coupled to Alexa 546 or 488, and used in a concentration of 4 μg/ml. To support the identification of nuclear boundaries all slices were stained with 4', 6-diamidino-2-phenylindole (DAPI, 10 mg/ml stock, diluted 1/5000). Negative controls were performed using pre-absorption with the antigen peptide and with omission of first respectively the secondary antibody (Suppl. Fig. 1).

Slices were analyzed with a Leica TCS SP2 laser-scanning microscope. Laser-power and amplification gain of the transporter-channels was kept constant over the different age samples. The borders of the z-axis for scanning stacks were determined via the DAPI staining. Single images in a stack were taken every 1 μm. Quantification was done with a custom-written MATLAB script for densitometric analysis. In brief, a cell was chosen in the calretinin-channel of a single z-plane with a clearly visible nucleus (confirmed in the DAPI-channel). The z-plane was selected where the cell analyzed had the maximal diameter. A line (region-of-interest, ROI) was drawn from the border of the cell membrane to the opposite cell membrane omitting the nucleus, based on the DAPI and calretinin channels. The intensity of the fluorescence in the transporter-channel (Fig. 5) was measured on the same z-plane. For each slide, 5 to 12 cells were analyzed. Since linear ROI had different length and thus different number of values per cell (E12: 29.9 ± 7, n = 266; E15: 34 ± 5.8, n = 570; E18: 39.2 ± 6.5, n = 709; P1: 52.3 ± 9.1, n = 814), all measured intensity profiles in the dataset were upsampled to the maximum ROI length in the dataset by linear interpolation for group data analysis. Accordingly, the fluorescence intensity values were also normalized to the maximum intensity values in the dataset. Measurements of different samples of the same age and transporter were pooled and the mean ± standard deviation was calculated.

3. Results

The aim of the study was to analyze the expression patterns of chloride transporters in the developing chicken auditory brainstem in order to better understand the molecular basis of the unusual chloride homeostasis in this system.

3.1. Classification of chloride transporters in the developing chicken

Our first approach was to identify which transporters out of a likely subset (Becker et al., 2003) of the large family of chloride transporters are expressed in the auditory brainstem and which of these show a regulation during development. The data obtained are based on 4 independent cDNA libraries each for 6 different developmental ages prepared out of 228 embryos and 5 P1 chicken. We grouped the transporters analyzed into three classes:

1. "Upregulated". Here, we found increasing expression and significant differences at different developmental ages.
2. "Not significantly different". The gene was present, but there were no significant differences detected at different developmental ages.
3. "Not expressed". The gene was either absent in the chicken genome or the relative expression compared to actin was a magnitude lower than in the other classes and/or a high number of amplifications did not reach the qPCR threshold.

The expression of the members of the "upregulated" class was further analyzed on the protein level with Western blot technique. The dataset is based on 4 independent lysates of each developmental age made out of 145 embryos and 8 P1 chicken.

To clarify in which cell-types and which cellular compartment the expression takes place, we performed immunohistochemical double-staining and subsequent densitometric analysis. This dataset is based on 124 embryos and 10 P1 chicken. We first present the upregulated genes.

3.2. NKCC1, KCC2 and KCC4 are upregulated

The expression of NKCC1 mRNA increased during development (Fig. 1A) starting with a relative expression to actin of around 0.02 at E7, E9 and E12 and doubling to about 0.04 at E15 and E18 and finally reaching 0.16 at P1. The ANOVA for NKCC1 mRNA expression showed a $p = 0.049$ at $df = 23$ and $F = 2.786$ and $N = 4$. The post-hoc Tukey-Cramer test showed significant differences between the expression at P1 and E7 and E9 ($\alpha < 0.05$). This developmental regulation of the expression was corroborated by the biochemical data. The expression of NKCC1 protein increased from about 0.3 at E7, E9 and E12 to about 0.6 at E15 and E18 and finally 0.8 at P1 (Fig. 2A). Thus, with both methods a strong increase in expression was found at around E12 and between E18 and P1. The ANOVA of the protein expression data was highly significant with $p = 8.39 \times 10^{-7}$ ($df = 23$, $F = 20.15$, $N = 4$). The post-hoc test showed significant differences between P1 and E7, E9, E12 ($\alpha < 0.01$), between E18 and E7, E9, E12 ($\alpha < 0.01$) and between E15 and E7, E9, E12 ($\alpha < 0.05$).

The mRNA expression of KCC2 increased more than 13-fold from E7 to P1. The initial expression at E7 and E9 was about 0.02 and rose at E15 and E18 to about 0.1. It finally reached 0.27 at P1 showing a biphasic increase similar to the expression of NKCC1 (Fig. 1B). The ANOVA for KCC2 mRNA had a $p = 0.0017$ at $df = 23$ and $F = 6.15$ and $N = 4$. The post-hoc Tukey-Cramer showed significant differences between the expression at P1 and E7 ($\alpha < 0.01$) and P1 and E9 ($\alpha < 0.05$). Expression at E15 and E18 was significantly different from E7 ($\alpha < 0.05$). The biochemical data confirmed these findings (Fig. 2B). The protein expression started at E7 and E9 below 0.7, rose at E12 to about 1.8, and finally reached about 3.0 from E15 on. The expression pattern still showed a steep increase around E12, but lacked an increase between E18 and P1. The ANOVA for KCC2 protein had a $p = 6.72 \times 10^{-4}$ ($df = 23$, $F = 7.31$, $N = 4$). The post-hoc Tukey-Cramer showed significant differences between the expression at P1 and E7, E9 ($\alpha < 0.05$) and between E15 and E7, E9 ($\alpha < 0.05$). Expression at E18 was significantly different from E7, E9 ($\alpha < 0.01$).

The mRNA expression of KCC4 was upregulated as well during development, although to a lesser extent (4.5-fold, Fig. 1C). The expression started with 0.02 at E7 and increased continuously to 0.03 at E9, 0.06 at E12 and 0.07 at E15. At E18 it decreased to 0.04 (not significantly different). At P1 the expression reached 0.09. The ANOVA for KCC4 mRNA expression showed a $p = 0.041$ at $df = 23$ and $F = 2.952$ and $N = 4$. The post-hoc Tukey-Cramer test showed a significant difference only between the expression at P1 and E7 ($\alpha < 0.05$). The biochemical data showed a similar pattern, although

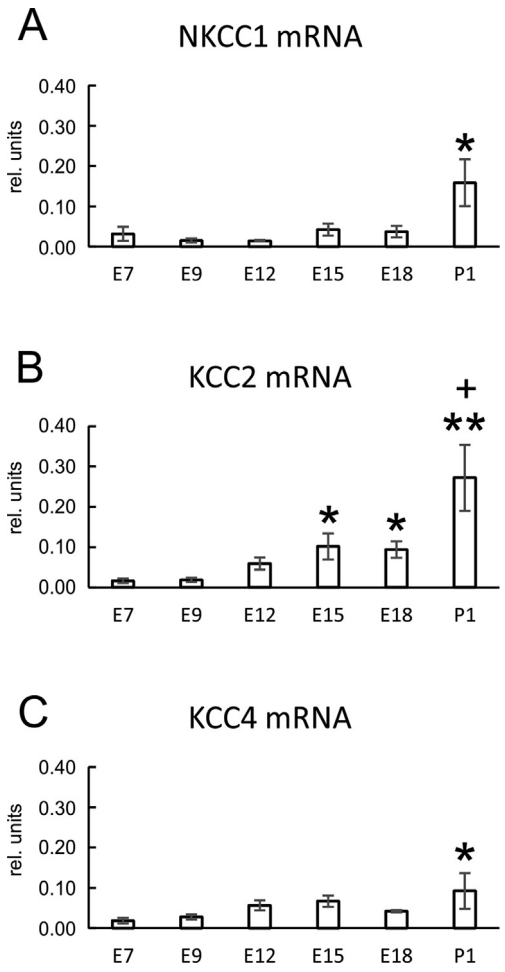

Fig. 1. Quantification of mRNA expression of NKCC1, KCC2 and KCC4. The mRNA expression of those three transporters shows a regulation during development. Bars show relative expression normalized to actin expression depending on developmental age. (A) NKCC1 mRNA expression is low up to E18 and shows a strong and significant increase at P1. (B) KCC2 mRNA expression increases during development as well. Steep increases are found between E12 and E15 with a plateau of expression at E15 and E18 and a second more prominent increase of expression between E18 and P1. (C) KCC4 shows an increase of mRNA expression during development with a less prominent but significant peak of expression at P1.
Asterisks: significant to E7, cross: significant to E9, one symbol: $p < 0.05$, two symbols: $p < 0.01$.

the relative amount of protein was increasing rather continuously from about 0.2 at E7 to about 0.4 at P1 (Fig. 2C). The ANOVA of the protein expression data had a $p = 9.32 \times 10^{-5}$ ($df = 23$, $F = 10.19$, $N = 4$). The post-hoc test showed significant differences between P1 and E7, E9, E12, E15 ($\alpha < 0.01$) and between E18 and E7, E9, E12 ($\alpha < 0.05$). The second outward transporter, KCC4 was expressed at lower levels than KCC2, only 1/3 of the mRNA and 1/7 of the protein signal. Due to the amount of expression and the level of regulation during development, we focused our study on NKCC1 and KCC2 and to a lesser extent on KCC4.

3.3. Relation of NKCC1 and KCC2

To clarify the relation of NKCC1 and KCC2 expression levels we compared the expression time course for both transporters during development in the auditory brainstem and the optic tectum (as control with a classical, hyperpolarizing GABAergic inhibition). The relative ratio of KCC2 to NKCC1 mRNA expression in the auditory brainstem showed a higher expression of NKCC1 at E7 (ratio 0.18), similar levels of both transporters at E9 (ratio 1.1) and thereafter an excess of KCC2 with a maximum at E12 (ratio 3.3; Fig. 3). From there on the slope of the curve flattened (E15: ratio 2.8; E18: ratio 2.6) up to the time of hatching (P1: 1.9). In contrast, in the optic tectum the expression ratio starts even more strongly in favor of NKCC1 (ratio 0.09) at E7. As in the auditory brainstem the expression ratio in the tectum shifts to higher values for KCC2 (E9: 0.34; E12: 1.4; E15: 4.8; E18: 3.0). At P1 we found 7.9 times more KCC2 mRNA expression than NKCC1. A two-tailed *t*-test of NKCC1 expression between auditory brainstem and tectum at P1 showed no significant difference (brainstem: 0.16 ± 0.06; tectum: 0.13 ± 0.03; $p = 0.525$; $N = 4$). In contrast, the expression of KCC2 at P1 is significantly different between brainstem and tectum (brainstem: 0.27 ± 0.08; tectum: 1.5 ± 0.46; $p = 0.036$; $N = 4$).

3.4. Shifts of localizations of NKCC1 and KCC2 during development

An essential prerequisite for ion transporters to be functional is the translocation to the membrane. Therefore, we performed immunohistochemistry in cells of Nucleus magnocellularis to study the location of the transporters. Neuronal identity was established with a double-staining against calretinin. Boundaries of the nuclei were determined using DAPI staining in comparison with Nissl-stained slices. The fluorescence intensity of transporter staining was measured for neurons in confocal planes.

While our resolution is not sufficient to prove a localization in the membrane, it clearly shows that at E12 the proteins of NKCC1 and KCC2 were localized at the rim of the cells with a distinct cytosolic component still detectable (Fig. 4A, E and Fig. 5A and B). During later stages of development (E15 and E18) the localization to the outer rim of the cells increased whereas the cytosolic component decreased (Fig. 4B–D and F–H and Fig. 5A and B). An additional strong cytosolic expression was detected again at P1 (Fig. 4D, H and Fig. 5A and B).

3.5. KCC4 predominantly expressed in glial cells

The expression pattern of KCC4 in neurons was different to that of NKCC1 and KCC2. An expression with a quite diffuse cytosolic component was first detected at E12 (Fig. 4I and J and Fig. 5C). The KCC4 staining still showed a distinct cytosolic component at E15 (Fig. 4J), although, hole-like structures with no staining surrounded by strong KCC4 staining appeared at this developmental stage. From E18 on there was a reticular-like strong staining for KCC4, encircling holes of absent staining (Fig. 4K). This continued to P1, although a weak cytosolic component in the neuronal somata reappeared (Fig. 4L). This staining pattern was reflected in the profiles by shift of the staining to the most outer rim of the neuronal diameter analyzed (Fig. 5C). The strong reticular-like KCC4 staining around hole-like structures suggested a predominantly non-neuronal expression and led to the hypothesis that KCC4 may be expressed in glia cells. Indeed, immunofluorescence for KCC4 was co-localized with GFAP and PLP at E15 and P1 (Fig. 6), supporting the hypothesis underlying the tests. By contrast, double staining of the chloride transporters with glial markers (GFAP for astrocytes and PLP for oligodendrocytes) revealed no co-localization of NKCC1 and KCC2 with glial markers (not shown).

3.6. KCC1, CCC6 and AE3 are not regulated

KCC1, CCC6 and AE3 did not show significant differences in their expressions at the different developmental ages. The ANOVA for KCC1 showed a $p = 0.726$ ($df = 23$, $F = 0.568$, $N = 4$). The expression at E7 was as high as at P1 but lower from E9 to E18. The mean expression was 0.055 (Fig. 7A). The ANOVA for CCC6 had a $p = 0.785$

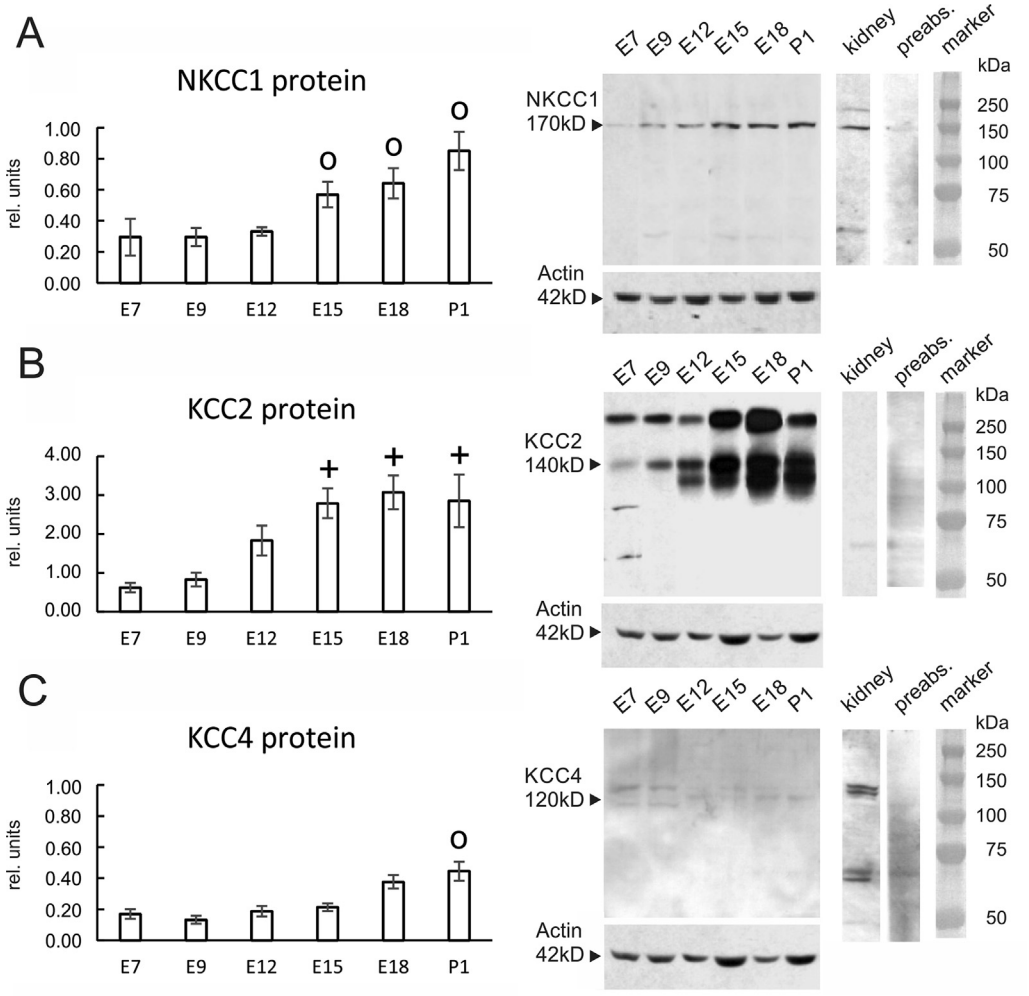

Fig. 2. Quantification of protein expression of NKCC1, KCC2 and KCC4. The regulation of the protein expression is similar to the mRNA expression during development. Bars in the left panel show relative expression normalized to actin expression depending on developmental age. Images on the right show representative blots for the expression of the transporters from E7 to P1. Target bands are indicated by arrows with the designated size of the protein. Blots below the main blots show actin expression. Additional lanes on the right show expression in kidney, neutralization of the primary antibody with antigen peptide and size marker. (A) NKCC1 protein is expressed low at E7 to E9 and increases continuously from E15 to P1 mimicking the mRNA expression pattern. NKCC1 is detected as a single band of 170 kD (arrow). At the same molecular weight, a band appears for kidney lysate. After pre-absorbing the antibody with peptides of its specific antigen site no staining at 170 kD is visible. (B) KCC2 protein expression increases from E9 on and reaches a plateau from E15 on lacking the strong increase seen in mRNA expression. Note the four times higher scale in relative expression compared to A and C. KCC2 is detected as a broad band at 140 kD (arrow) with a side band at higher molecular weight (~280–300 kD). These are possibly dimers. As expected, the neuron specific KCC2 is absent in kidney lysates. After pre-absorption of the antibody with the antigenic peptide, no staining is detectable. (C) KCC4 protein expression increases during development reflecting the expression profile seen for mRNA expression. KCC4 is detected at 120 kD (arrow) in brainstem lysates. In kidney lysates, we find a double band at the corresponding molecular weight as well as at much lower molecular weight. No staining is detected after pre-absorption of the antibody.
Cross: significant to E9, circle: significant to E12, one symbol: $p < 0.05$, two symbols: $p < 0.01$.

($df = 23$, $F = 0.482$, $N = 4$). The mean expression was 0.036 (Fig. 7B). The ANOVA for AE3 revealed a $p = 0.383$ ($df = 23$, $F = 1.124$, $N = 4$) with a mean expression of 0.096 (Fig. 7C).

3.7. NKCC2 and CCC9 are not expressed

The expression of NKCC2 was so low that in 54% of the amplifications it did not reach the baseline threshold. This was assigned as “below threshold”. When an expression was detectable, it was usually two orders of magnitude lower than the expression of all the other transporters (Fig. 7D). The expression of CCC9 was also close to the detection threshold with 6.6% of all amplifications not reaching the baseline threshold. The mean cDNA concentration of CCC9 was 15 times lower than the lowest values of the rest of the transporters (Fig. 7E). Positive controls were done with cDNA libraries derived from optic tectum and kidney (both P1).

4. Discussion

We here provide a developmental study of expression profiles of several chloride transporters in the chicken. The transporters NKCC1, KCC2 and KCC4 are significantly upregulated in the auditory brainstem of developing chicken. The expression increased on both mRNA and protein levels. After E9, there was always a higher expression of KCC2 than NKCC1. The ratio of KCC2 to NKCC1 mRNA expression in the optic tectum (control) was several fold higher compared to the auditory brainstem. NKCC1 and KCC2 immunosignals shifted from a more cytosolic location to the outer rim of the cells suggesting a transport to the cell membrane during development. KCC4 was localized predominantly in astrocytes and oligodendrocytes. In the following, we discuss these results with respect to 1) results in other species, 2) the relation of NKCC1 and KCC2, 3) a possible role of KCC2 in structural development of auditory

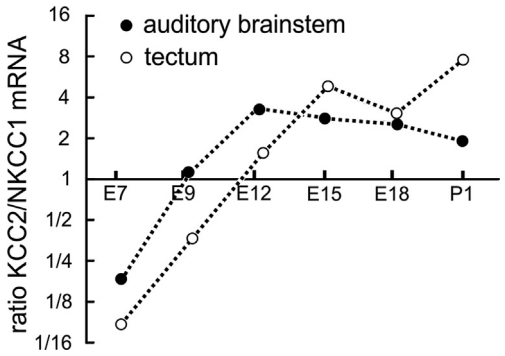

Fig. 3. Relative expression of chloride transporters in auditory brain stem and optic tectum during chick development. (A) The ratio of KCC2 to NKCC1 mRNA expression shows that early in development there is more NKCC1 than KCC2 expression in both tissues. Around E9/E12 this changes and the expression of KCC2 increases much stronger than for NKCC1. After E15 the KCC2-NKCC1- ratio is higher in tectum than in auditory brainstem. Although from this stage on KCC2 shows higher expression than NKCC1, this difference is more pronounced in tectum than in auditory brainstem. White circles: KCC2/NKCC1 expression ratio of tectum. Black circles: KCC2/NKCC1 expression ratio of auditory brain stem.

brainstem synapses, and 4) the possible effect of KCC2 on the chloride equilibrium potential and functional consequences for auditory information processing.

4.1. Comparison to other species

Previous studies showed that NKCC1 is not expressed in the rat lateral superior olive (LSO) at birth (P0), but was detected at P6 and P16 (Balakrishnan et al., 2003). At the time points where NKCC1 expression was found, glycinergic chloride currents were already hyperpolarizing (Kandler and Friauf, 1995). The AE3 transporter served a likely candidate for the early inward transport and was found to be expressed in the LSO at early age (Becker et al., 2003). However, AE3 knockout mice retained E_{Cl} values 35 mV more positive than their resting membrane potential (Hentschke et al., 2006). In contrast to the situation in the rat, we found NKCC1 to be expressed in the chicken from early ages on. One reason for the difference in expression onset might be that chickens are precocial animals, while rats are altricial. This is reflected in a time course of the auditory development that is drastically different between the chicken and mammals like mice and rat. For example, the time of hearing onset for chicken is reported as early as around E16 (Jones et al., 2006) whereas for mice it is P10-12 (Mikaelian and Ruben, 1965; Ehret, 1983) and for rats it is P11 -13 (Uziel et al., 1981; Ehret, 1983; Geal-Dor et al., 1993).

The NKCC1 expression increased during development rendering this transporter a likely candidate to be responsible for the chloride transport into auditory brainstem cells. The expression of the other typical chloride transporters was similar for rat and chicken. Neither NCC nor NKCC2 were detectable in the brainstem of rats or chicken, while AE3 was expressed in the brainstems of both species and could contribute to the chloride influx (Balakrishnan et al., 2003; Becker et al., 2003). KCC3 was absent in the chicken. This is consistent with genomic data from both the chicken and the zebra finch (Gagnon and Delpire, 2013). Furthermore, we found KCC2 and KCC4 expression from early developmental stage on, similar to data obtained in rat. KCC4 is most likely not expressed in chicken brainstem neurons but predominantly in surrounding glia cells. The situation in the rat is unclear in this respect, since Becker et al. (2003) did not distinguish between glia and neurons when employing *in situ* hybridization. KCC4 was also found in teleost fish, birds and mammals but was absent in amphibians (Xenopus) and reptiles (Anolis) (Gagnon and Delpire, 2013). The functional role of KCC4 in glia cells remains to be studied.

Membrane localization is essential for correct transport function. While the resolution of our data is not sufficient to prove localization of the transporters in the membrane, we clearly observed an increasing recruitment of NKCC1 and KCC2 to the outer rim of the neurons during development. We take this as an indication for membrane localization. We like to mention here that there is still a caveat concerning the specificity of the NKCC1 antibody. We performed pre-absorption tests with the antigenic peptide, checked for the lack of sequence identity with other members of the CCCs in the peptide and performed negative tests omitting 1st or 2nd antibody. However, since there are no NKCC1 knock-out chicken available, the final proof of specificity is impossible.

The additional cytosolic component we found at P1 could reflect the steep increase in expression seen in Western blot and qPCR. This might be a sign of a high turn-over rate in mature neurons (Rivera et al., 2004). However, there was also a methodological difference that could have influenced the binding efficiency of the antibodies, since P1 animals were perfused whereas the brainstems of earlier ages were only immersion fixed.

4.2. Relation of NKCC1 and KCC2

We were puzzled by our observation that both transporters, the inward NKCC1 as well as the outward KCC2 transporter increased their expression levels during development with highest expression occurring at P1 (last age analyzed). Several studies in the auditory brainstem report the chloride reversal potential to remain more positive than the resting potential even at post-hatch stages (Hyson et al., 1995; Monsivais et al., 2000; Monsivais and Rubel, 2001). Based on this, our initial hypothesis was a higher expression of NKCC1 at all developmental ages and a low or absent expression of KCC2 in later ages. However, data from rat auditory brainstem had already shown that KCC2 expression was much more prominent than NKCC1 expression during development (Balakrishnan et al., 2003). Our data are consistent with these data from the rat. The expression of the transporters might not be an accurate measure for transport efficacy and chloride turnover. NKCC1 can transport two chloride ions per cycle, whereas KCC2 transports only one, rendering NKCC1 potentially twice as effective. Furthermore, several post-translational modifications that regulate the transport rate have been described. This ranges from oligomerization of KCC2 (Blaesse et al., 2006), activity-dependent regulation of KCC2 function (Huberfeld et al., 2007), inhibition of KCC2 transport activity by zinc (Hershfinkel et al., 2009) and regulation due to phosphorylation. Especially the latter is of great interest since phosphorylation of NKCC1 and KCC2 regulates the transport rate reciprocally. Specifically, the transport rate of NKCC1 after threonine phosphorylation is increased and the transport rate of KCC2 after phosphorylation of serine and threonine sites is decreased (Rinehart et al., 2009; Kahle et al., 2010). Recent studies have shown that KCC2 has five phosphorylation sites allowing a complex regulation of its activity by integrating different signaling pathways (Cordshagen et al., 2018). On the other hand, KCC2 is the only member of the KCCs that is constitutively active and does not need to be activated due to hypotonicity (Mercado et al., 2006).

When comparing the relative mRNA expression of KCC2 to NKCC1 between auditory brainstem and optic tectum a much higher excess of KCC2 was demonstrated in optic tectum. Notably, GABAergic inhibition is hyperpolarizing in the optic tectum (reviewed in Binns, 1999). This could be interpreted as KCC2 being much less active than NKCC1 in tectum and, thus, the need of a huge excess of KCC2 protein to reach a E_{Cl} lower than resting membrane potential.

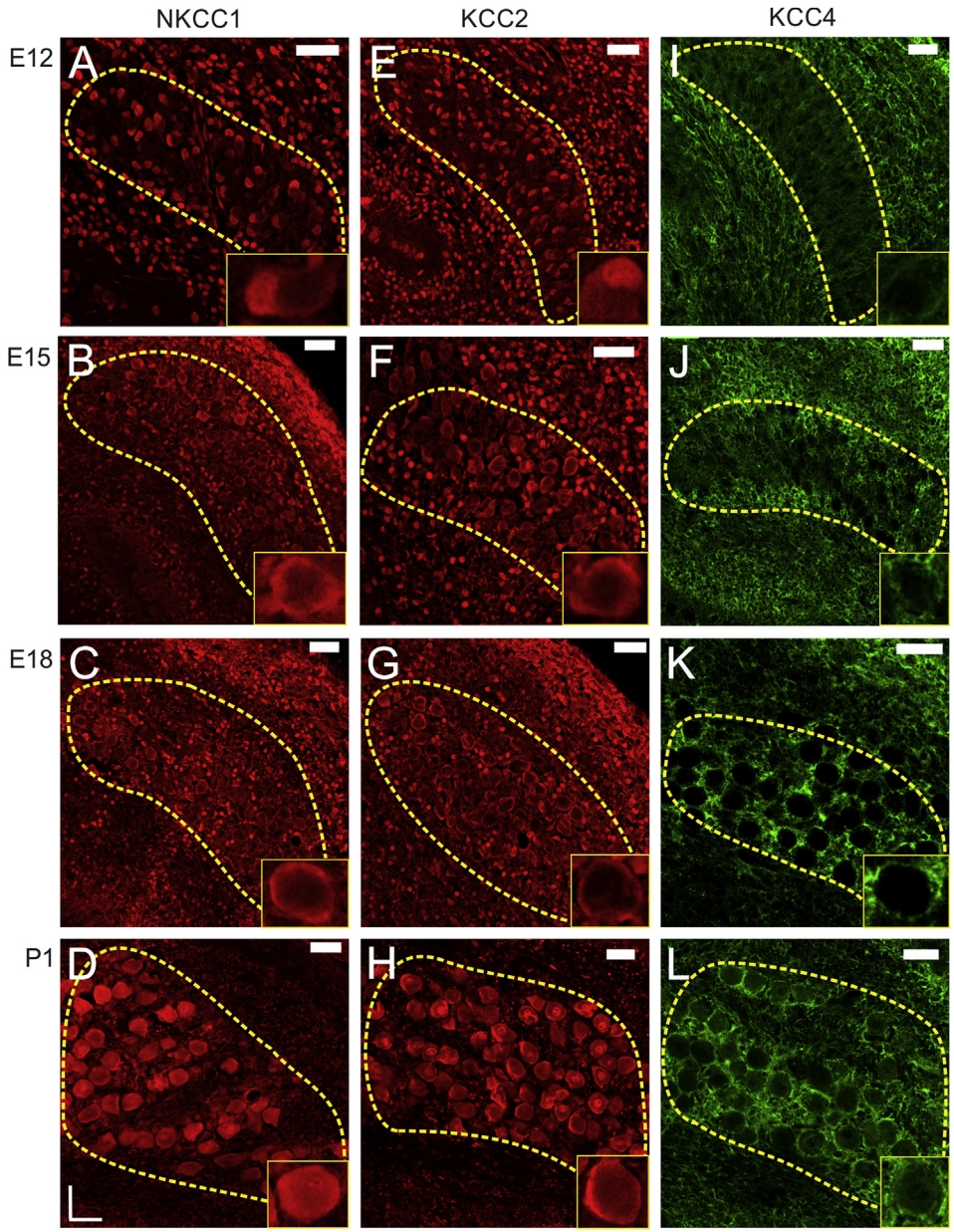

Fig. 4. Photomicrographs of immunofluorescent staining of NKCC1, KCC2 and KCC4 in Nucleus magnocellularis at E12, E15, E18 and P1. Neuronal identity was confirmed using a double-staining against calretinin. Boundaries of the Nuclei were determined with DAPI staining in comparison with Nissl-stained slices. Inlays show a typical cell in detail. Dotted lines indicate the borders of the nuclei. At E12 the distribution of (A) NKCC1, (E) KCC2 and (I) KCC4 appears still diffuse. The staining for KCC4 seems to be much weaker than for the other two transporters. From E15 on NKCC1 seem to be recruited more and more to the membrane (B, C). At P1 NKCC1 is still located at the membrane, but an additional cytosolic component appears (D). A similar pattern is seen for KCC2 (F–H). The KCC4 staining has at E15 still a distinct cytosolic component (J). From E18 on there is a reticular-like strong staining for KCC4, encircling holes of absent staining (K). This continued to P1, although a weak cytosolic component seems to reappear (L). The strong reticular-like KCC4 staining around the hole-like structures suggests a non-neuronal expression. Scale bar is 40 μm, dorsal is up and lateral is right.

In this developmental study, we neglected the chloride transport of KCC1 and AE3 because both are expressed at similar levels and are not regulated during development. A role of AE3 in GABA receptor-mediated lower seizure thresholds and epilepsy is discussed in the literature usually focusing on the bicarbonate transport rather than the chloride transport (reviewed in Rahmati et al., 2018). We speculate that KCC1 and AE3 are involved in basal chloride homeostasis e.g. volume regulation, but cannot exclude a potential role in GABAergic transmission.

4.3. A possible role of KCC2 in structural development of auditory brainstem synapses

NKCC1 and KCC2 expression increased at two distinct time points in development: between E12 and E15 and at P1. At E13, NMDA receptor driven EPSC can be evoked (Lu and Trussell, 2007). Auditory nerve fibers contact the NM neurons and primordial spontaneous bursting activity in the auditory pathway has just started to occur (Jones et al., 2001). Sound-driven responses are still

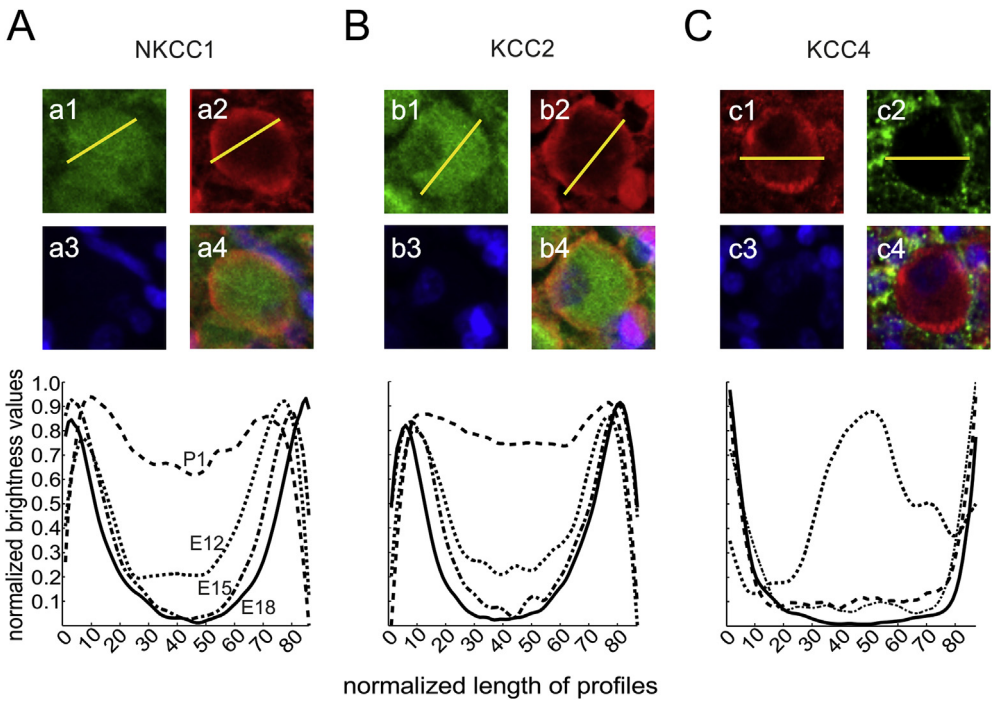

Fig. 5. Quantification of the localization of the staining. The normalized brightness values of a densitometric measurement along a line through sampled cells avoiding the cellular nucleus are plotted against the normalized length of the measured line. The line spans the complete width of the cell based on the calretinin staining. This is illustrated in the pictures labelled with small letters. These are sample cells from stage E18. The pictures show calretinin expression (1), transporter expression (2) nuclear staining (3) and the merge of all three channels (4). The yellow line in 1 and 2 designates a typical line of interest. (A) From E12 to E18 the amount of NKCC1 staining seen in the cytosol decreases and the main part of the staining shifts to the rim. The shape of the profiles with visible peaks at the rim suggests a localization to the membrane. The width of the cells seems to be slightly overestimated. At P1 an additional cytosolic component of the staining appears. (B) The same is true for the KCC2 staining. (C) The KCC4 staining profile starts at E12 with a cytosolic component and a lack of staining at the rim. However, from E15 on up to P1 the bulk of the staining is localized at the most outer part of the rim of the line scan. The profiles form troughs with no visible peaks. This led to the hypothesis that the staining is not in the calretinin-positive neurons, but in the surrounding glia cells. (For interpretation of the references to colour in this figure legend, the reader is referred to the Web version of this article.)

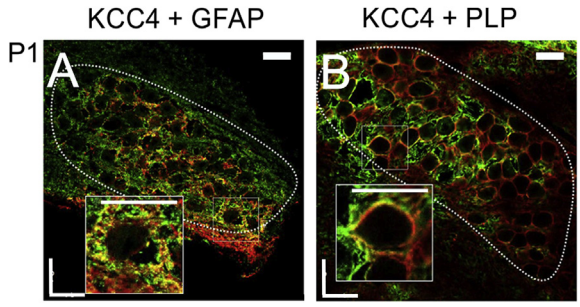

Fig. 6. Double-staining for KCC4 and glial markers at P1. (A) Nucleus magnocellularis stained for KCC4 (red) and the astrocyte-marker GFAP (green). (B) Staining for KCC4 (red) and the oligodendrocyte-marker PLP (green). Yellow spots (Arrows) designate double-staining. Small squares show origin of the magnification shown in the big squares. Scale bars: 40 μm. Dorsal is up and lateral is right. (For interpretation of the references to colour in this figure legend, the reader is referred to the Web version of this article.)

mostly absent or only occur to extreme stimulus levels (Jones et al., 2006). In rodents, this physiological state would roughly correspond to the end of the first postnatal week (Limb and Ryugo, 2000; Isaacson and Walmsley, 1995; Sonntag et al., 2009). Therefore, we conclude that E13 in the chicken corresponds to P1−P8 of rodents. The increase of expression at P1 in our data is close in time to functional maturation of air-driven sound processing in chicken with synaptically driven activity increasing dramatically (Jones et al., 2006). Moreover, at E15 a massive restructuring of NM neurons takes place (Goyer et al., 2015). The latter authors observed a retraction of dendrites on the one hand, while on the other hand synapses form directly at the soma. Li et al. (2007) and Fiumelli et al. (2013) demonstrated a role of KCC2 in the formation of dendritic spines that is independent on its ability to transport ions. Although chicken auditory brainstem neurons are spineless, the interaction of the C-terminus of KCC2 with the actin-associated protein 4.1N can affect actin-depolymerization and AMPA receptor recruitment to synapses (Gauvain et al., 2011). Further, KCC2 regulates actin dynamics via interaction with the guanine nucleotide exchange factor β-PIX (Llano et al., 2015). This is potentially a mechanism to reshape dendrites and boost synapse maturation. This structural reorganization also leads to an increase in activity (Goyer et al., 2015). These changes in synaptic activity can upregulate the expression of brain-derived neurotrophic factor (BDNF, Zafra et al., 1991), and BDNF may then in turn cause an upregulation of KCC2 (Aguado et al., 2003). We speculate that in this way a loop exists in the auditory brainstem that drives structural and functional maturation.

4.4. Possible effect of KCC2 on the chloride equilibrium potential and functional consequences

The E_{Cl} influences a number of physiological phenomena. For example, early in embryonic development, many neurons in mammalian neocortex and hippocampus show a high E_{Cl}, and the activation of $GABA_A$ receptor channels leads to a chloride efflux and a depolarization. This generates primitive patterns of network activity that synchronizes gene expression and synaptogenesis to shape functional units in developing cortical networks (Ben-Ari, 2002; Owens and Kriegstein, 2002; Reimondo et al., 2017). Later

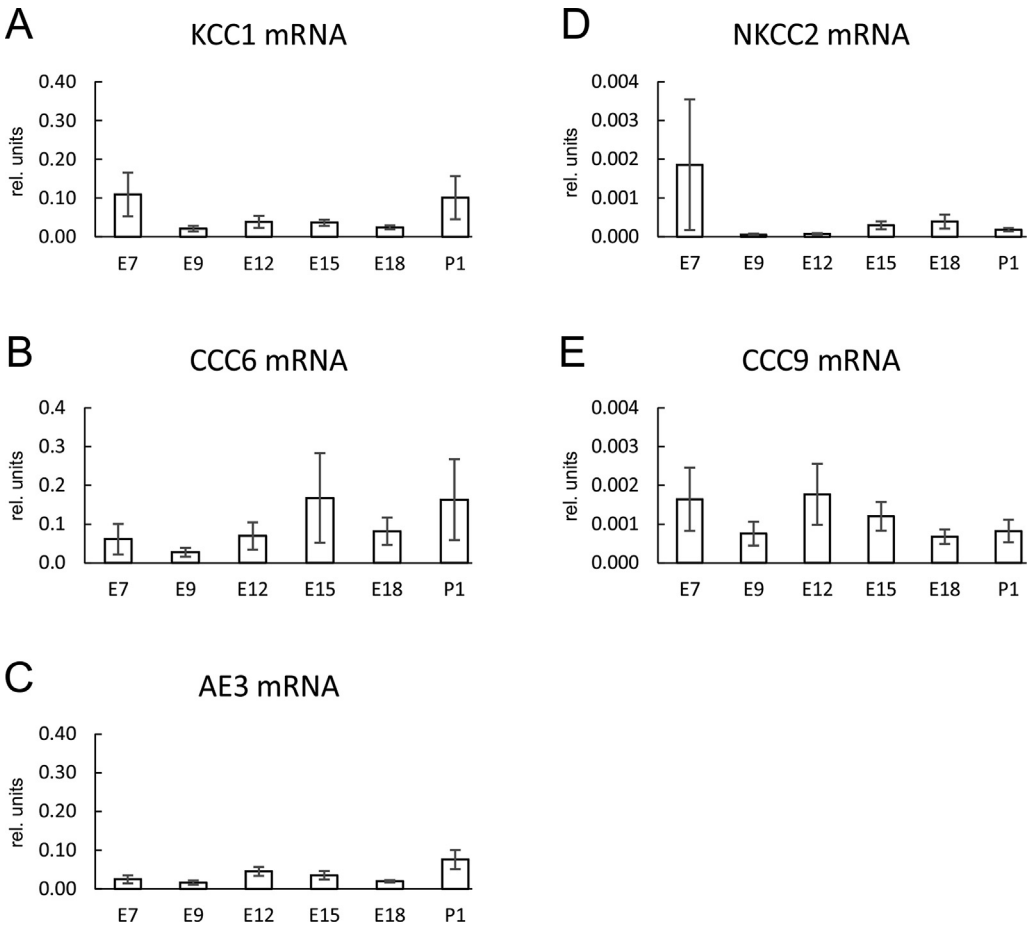

Fig. 7. KCC1, CCC6 and AE3 expression was not significantly regulated. NKCC2 and CCC9 expression was close to threshold. (A) KCC1 showed at most time points analyzed a low expression with no distinct trend in expression levels. No significant differences were found. (B) The orphan transporter CCC6 shows a highly variable expression pattern with no significant differences between the six developmental ages. (C) The expression of the only transporter not belonging to the SLC12 family, AE3, is low in all stages analyzed and shows no distinct pattern. No significant differences were found. (D) NKCC2 and (E) CCC9 mRNA is expressed an order of magnitude lower than all other transporters analyzed. No distinct expression patterns are obvious and no significant differences were found. In 54% of the amplifications of NKCC2 and in 6.6% of the amplifications of CCC9 the threshold was not reached, which can be interpreted as "not expressed".

in development, the E_{Cl} shifts to lower values so that the opening of $GABA_A$ receptor channels causes an influx of chloride and KCC2 is held responsible for the hyperpolarizing effects of GABA (Hubner et al., 2001; Rivera et al., 1999; Woo et al., 2002). This membrane hyperpolarization is the basis of classical GABAergic inhibition (reviewed in Obata, 2013). GABAergic responses remain depolarizing in post-hatch NM and NL neurons (Hyson et al., 1995; Monsivais et al., 2000; Monsivais and Rubel, 2001; Tang et al., 2009). The resulting shunting inhibition is more powerful than conventional hyperpolarizing inputs in the same neurons (Howard et al., 2007; Howard and Rubel, 2010). This inhibition underlies the improvement of coding of interaural time differences by enhancing the fidelity of neuronal phase locking in NM, to provide a gain control for the excitatory inputs from NM to NL and to sharpen the coincidence detection window in NL neurons (Kuba et al., 2002). Since sound localization depends on microsecond precision, a tight control of the E_{Cl} and the resulting inhibition is of great importance. We speculate that KCC2 plays a role in a push-pull-regulation of intracellular chloride levels together with NKCC1. A regulation with two degrees of freedom increases flexibility in adjusting E_{Cl} allowing for a high dynamic range in gain control.

Thus, the upregulation of both NKCC1 and KCC2 in chicken auditory brainstem may reflect an adaptation for more flexibility and precision in the first nuclei of the avian auditory system.

Author contributions

TA, AK, KA and MW carried out the experiments. TK and JM helped with data analysis and data interpretation. MW and HW wrote the initial draft of the manuscript.

Author statement

Tobias Ackels, Andreas Kriebel, Katharina Kriebel: Methodology, Validation, Formal analysis, Investigation, Data curation, Visualization.

Thomas Künzel: Software, Validation, Formal analysis, Data curation, Visualization, Writing – Review & Editing.

Jörg Mey: Methodology, Validation, Formal analysis.

Marcus Wirth: Conceptualization, Methodology, Validation, Formal analysis, Data curation, Writing – Original draft, Writing – Review & Editing, Visualization, Supervision, Project administration.

Hermann Wagner: Resources, Writing – Original draft, Writing – Review & Editing, Funding aquisition.

Declaration of competing interest

The authors declare no competing interests.

Acknowledgements

We thank Stefanie Kurth for excellent technical help and Lea Dewenter for glial immunostaining.

Appendix A. Supplementary data

Supplementary data to this article can be found online at https://doi.org/10.1016/j.heares.2020.108013.

Abbreviations

AE	anion exchanger family
CCC	Cation chloride cotransporters
E	embryonic day
E_{Cl}	chloride equilibrium potential
GABA	γ-amino butyric acid
ITD	interaural time difference
KCC	potassium chloride co-transporter
LSO	lateral superior olive
NA	nucleus angularis
NKCC	sodium-potassium chloride co-transporter
NL	nucleus laminaris
NM	nucleus magnocellularis
SLC12	family of chloride transporters
SON	superior olivary nucleus

References

Adragna, N.C., Di Fulvio, M., Lauf, P.K., 2004. Regulation of K-Cl cotransport: from function to genes. J. Membr. Biol. 201, 109–137. Erratum in: J. Membr. Biol. 210, 213.

Aguado, F., Carmona, M.A., Pozas, E., Aguiló, A., Martínez-Guijarro, F.J., Alcantara, S., Borrell, V., Yuste, R., Ibañez, C.F., Soriano, E., 2003. BDNF regulates spontaneous correlated activity at early developmental stages by increasing synaptogenesis and expression of the K+/Cl- co-transporter KCC2. Development 130, 1267–1280.

Balakrishnan, V., Becker, M., Löhrke, S., Nothwang, H.G., Güresir, E., Friauf, E., 2003. Expression and function of chloride transporters during development of inhibitory neurotransmission in the auditory brainstem. J. Neurosci. 23, 4134–4145.

Becker, M., Nothwang, H.G., Friauf, E., 2003. Differential expression pattern of chloride transporters NCC, NKCC2, KCC1, KCC3, KCC4, and AE3 in the developing rat auditory brainstem. Cell Tissue Res. 312, 155–165.

Ben-Ari, Y., 2002. Excitatory actions of GABA during development: the nature of nurture. Nat. Rev. Neurosci. 3, 728–739.

Blaesse, P., Guillemin, I., Schindler, J., Schweizer, M., Delpire, E., Khiroug, L., Friauf, E., Nothwang, H.G., 2006. Oligomerization of KCC2 correlates with development of inhibitory neurotransmission. J. Neurosci. 26, 10407–10419.

Code, R.A., Churchill, L., 1991. GABAA receptors in auditory brainstem nuclei of the chick during development and after cochlea removal. Hear. Res. 54, 281–295.

Cordshagen, A., Busch, W., Winklhofer, M., Nothwang, H.G., Hartmann, A.M., 2018. Phosphoregulation of the intracellular termini of K^+-Cl^- cotransporter 2 (KCC2) enables flexible control of its activity. J. Biol. Chem. 293, 16984–16993.

Daigle, N.D., Carpentier, G.A., Frenette-Cotton, R., Simard, M.G., Lefoll, M.H., Noël, M., Caron, L., Noël, J., Isenring, P., 2009. Molecular characterization of a human cation-Cl-cotransporter (SLC12A8A, CCC9A) that promotes polyamine and amino acid transport. J. Cell. Physiol. 220, 680–689.

Ehret, G., 1983. Development of hearing and response behavior to sound stimuli: behavioral studies. In: Romand, R. (Ed.), Development of Auditory and Vestibular Systems. Academic, New York, pp. 211–237.

Fiumelli, H., Briner, A., Puskarjov, M., Blaesse, P., Belem, B.J., Dayer, A.G., Kaila, K., Martin, J.L., Vutskits, L., 2013. An ion transport-independent role for the cation-chloride cotransporter KCC2 in dendritic spinogenesis in vivo. Cerebr. Cortex 23, 378–388.

Friauf, E., Rust, M.B., Schulenborg, T., Hirtz, J.J., 2011. Cloride cotransporters, chloride homeostasis, and synaptic inhibition in the developing auditory system. Hear. Res. 279, 96–110.

Funabiki, K., Koyano, K., Ohmori, H., 1998. The role of GABAergic inputs for coincidence detection in the neurones of nucleus laminaris of the chick. J. Physiol. 508, 851–869.

Gamba, G., Saltzberg, S.N., Lombardi, M., Miyanoshita, A., Lytton, J., Hediger, M.A., Brenner, B.M., Hebert, S.C., 1993. Primary structure and functional expression of a cDNA encoding the thiazide-sensitive, electroneutral sodium-chloride cotransporter. Proc. Natl. Acad. Sci. U.S.A. 90, 2749–2753.

Gagnon, K.B., Delpire, E., 2013. Physiology of SLC12 transporters: lessons from inherited human genetic mutations and genetically engineered mouse knockouts. Am. J. Physiol. Cell Physiol. 304, 693–714.

Gauvain, G., Chamma, I., Chevy, Q., Cabezas, C., Irinopoulou, T., Bodrug, N., Carnaud, M., Lévi, S., Poncer, J.C., 2011. The neuronal K-Cl cotransporter KCC2 influences postsynaptic AMPA receptor content and lateral diffusion in dendritic spines. Proc. Natl. Acad. Sci. U.S.A. 108, 15474–15479.

Geal-Dor, M., Freeman, S., Li, G., Sohmer, H., 1993. Development of hearing in neonatal rats: air and bone conducted ABR thresholds. Hear. Res. 69, 236–242.

Goyer, D., Fensky, L., Hilverling, A.M., Kurth, S., Kuenzel, T., 2015. Expression of the postsynaptic scaffold PSD-95 and development of synaptic physiology during giant terminal formation in the auditory brainstem of the chicken. Eur. J. Neurosci. 41, 1416–1429.

Hamburger, V., Hamilton, H.L., 1951. A series of normal stages in the development of the chick embryo. J. Morphol. 88, 49–92.

Hentschke, M., Wiemann, M., Hentschke, S., Kurth, L., Hermanns-Borgmeyer, I., Seindbecher, T., Jentsch, T.J., Hübner, C.A., 2006. Mice with a targeted disruption of the CL-/HCO3-exchanger AE3 display a reduced seizure threshold. Mol. Cell Biol. 26, 182–191.

Hershfinkel, M., Kandler, K., Knoch, M.E., Dagan-Rabin, M., Aras, M.A., Abramovitch-Dahan, C., Sekler, I., Aizenman, E., 2009. Intracellular zinc inhibits KCC2 transporter activity. Nat. Neurosci. 12, 725–727.

Howard, M.A., Burger, R.M., Rubel, E.W., 2007. A developmental switch to GABAergic inhibition dependent on increases in Kv1-type K+ currents. J. Neurosci. 27, 2112–2123.

Howard, M.A., Rubel, E.W., 2010. Dynamic spike thresholds during synaptic integration preserve and enhance temporal response properties in the avian cochlear nucleus. J. Neurosci. 30, 12063–12074.

Hyson, R.L., Reyes, A.D., Rubel, E.W., 1995. A depolarizing inhibitory response to GABA in brainstem auditory neurons of the chick. Brain Res. 677, 117–126.

Hubner, C.A., Stein, V., Hermans-Borgmeyer, I., Meyer, T., Ballanyi, K., Jentsch, T.J., 2001. Disruption of KCC2 reveals an essential role of K-Cl cotransport already in early synaptic inhibition. Neuron 30, 515–524.

Isaacson, J.S., Walmsley, B., 1995. Receptors underlying excitatory synaptic transmission in slices of the rat anteroventral cochlear nucleus. J. Neurophys. 73, 964–973.

Jones, T.A., Jones, S.M., Paggett, K.C., 2001. Primordial rhythmic bursting in embryonic cochlear ganglion cells. J. Neurosci. 21, 8129–8135.

Jones, T.A., Jones, S.M., Paggett, K.C., 2006. Emergence of hearing in the chicken embryo. J. Neurophysiol. 96, 128–141.

Kahle, K.T., Rinehart, J., Lifton, R.P., 2010. Phosphoregulation of the Na-K-2Cl and K-Cl cotransporters by the WNK kinases. Biochim. Biophys. Acta (BBA) - Mol. Basis Dis. 1802, 1150–1158.

Kandler, K., Friauf, E., 1995. Development of glycinergic and glutamatergic synaptic transmission in the auditory brainstem of perinatal rats. J. Neurosci. 15, 6890–6904.

Kobayashi, S., Morgans, C.W., Casey, J.R., Kopito, R.R., 1994. AE3 anion exchanger isoforms in the vertebrate retina: developmental regulation and differential expression in neurons and glia. J. Neurosci. 14, 6266–6279.

Kuba, H., Koyano, K., Ohmori, H., 2002. Synaptic depression improves coincidence detection in the nucleus laminaris in brainstem slices of the chick embryo. Eur. J. Neurosci. 15, 984–990.

Kuo, S.P., Bradley, L.A., Trussell, L.O., 2009. Heterogeneous kinetics and pharmacology of synaptic inhibition in the chick auditory brainstem. J. Neurosci. 29, 9625–9634.

Llano, O., Smirnov, S., Soni, S., Golubtsov, A., Hotulainen, P., Medina, I., Nothwang, H.G., Rivera, C., Ludwig, A., 2015. KCC2 regulates actin dynamics in dendritic spines via interaction with β-PIX. J. Cell Biol. 209, 671–686.

Li, H., Khirug, S., Cai, C., Ludwig, A., Blaesse, P., Kolikova, J., Afzalov, R., Coleman, S.K., Lauri, S., Airaksinen, M.S., Keinänen, K., Khiroug, L., Saarma, M., Kaila, K., Rivera, C., 2007. KCC2 interacts with the dendritic cytoskeleton to promote spine development. Neuron 56, 1019–1033.

Limb, C.J., Ryugo, D.K., 2000. Development of primary axosomatic endings in the anteroventral cochlear nucleus of mice. JARO 1, 103–119.

Lu, T., Trussell, L.O., 2007. Development and elimination of endbulb synapses in the chick cochlear nucleus. J. Neurosci. 27, 808–817.

Mercado, A., Broumand, V., Zandi-Nejad, K., Enck, A.H., Mount, D.B., 2006. A C-terminal domain in KCC2 confers constitutive K^+-Cl^- cotransport. J. Biol. Chem. 281, 1016–1026.

Mikaelian, D., Ruben, R.J., 1965. Development of hearing in the normal Cba-J mouse: correlation of physiological observations with behavioral responses and with cochlear anatomy. Acta Otolaryngol. 59, 451–461.

Monsivais, P., Rubel, E.W., 2001. Accommodation enhances depolarizing inhibition in central neurons. J. Neurosci. 21, 7823–7830.

Monsivais, P., Yang, L., Rubel, E.W., 2000. GABAergic inhibition in nucleus magnocellularis: implications for phase locking in the avian auditory brainstem. J. Neurosci. 20, 2954–2963.

Müller, C.M., 1987. γ-Aminobutyric acid immunoreactivity in brainstem auditory nuclei of the chicken. Neurosci. Lett. 77, 272–276.

Obata, K., 2013. Synaptic inhibition and γ-aminobutyric acid in the mammalian central nervous system. Proc. Jpn. Acad. Ser. B Phys. Biol. Sci. 89, 139–156.

Ohmori, H., 2014. Neuronal specializations for the processing of interaural difference cues in the chick. Front. Neural Circ. 8, 47.

Owens, A.F., Kriegstein, A.R., 2002. Is there more to GABA than synaptic inhibition? Nat. Rev. Neurosci. 3, 715–727.

Payne, J.A., Stevenson, T.J., Donaldson, L.F., 1996. Molecular characterization of a

putative K-Cl cotransporter in rat brain. A neuronal-specific isoform. J. Biol. Chem. 271, 16245–16252.
Rahmati, N., Hoebeek, F.E., Peter, S., De Zeeuw, C.I., 2018. Chloride homeostasis in neurons with special emphasis on the olivocerebellar system: differential roles for transporters and channels. Front. Cell. Neurosci. 12, 101.
Reimondo, J.V., Richards, B.A., Woodin, M.A., 2017. Neuronal chloride and excitability — the big impact of small changes. Curr. Opin. Neurobiol. 43, 35–42.
Rinehart, J., Maksimova, Y.D., Tanis, J.E., Stone, K.L., Hodson, C.A., Zhang, J., Risinger, M., Pan, W., Wu, D., Colangelo, C.M., Forbush, B., Joiner, C.H., Gulcicek, E.E., Gallagher, P.G., Lifton, R.P., 2009. Sites of regulated phosphorylation that control K-Cl cotransporter activity. Cell 138, 525–536.
Rivera, C., Voipio, J., Payne, J.A., Ruusuvuori, E., Lahtinen, H., Laamsa, K., Pirvola, U., Saarma, M., Kaila, K., 1999. The K+/Cl- cotransporter KCC2 renders GABA hyperpolarizing during neuronal maturation. Nature 397, 251–255.
Rivera, C., Voipio, J., Thomas-Crusells, J., Li, H., Emri, Z., Sipilä, S., Payne, J.A., Minichiello, L., Saarma, M., Kaila, K., 2004. Mechanism of activity-dependent downregulation of theNeuron-specific K-Cl cotransporter KCC2. J. Neurosci. 4683–4691.
Sonntag, M., Englitz, B., Kopp-Scheinpflug, C., Rübsamen, R., 2009. Early postnatal development of spontaneous and acoustically evoked discharge activity of principal cells of the medial nucleus of the trapezoid body: an in vivo study in mice. J. Neurosci. 29, 9510–9520.
Tabor, K.M., Coleman, W.L., Rubel, E.W., Burger, R.M., 2012. Tonotopic organization of the superior olivary nucleus in the chicken auditory brainstem. J. Comp. Neurol. 520, 1493–1508.
Tang, Z.Q., Gao, H., Lu, Y., 2009. Control of a depolarizing GABAergic input in an auditory coincidence detection circuit. J. Neurophysiol. 102, 1672–1683.
Uziel, A., Romand, R., Marot, M., 1981. Development of cochlear potentials in rats. Audiology 20, 89–100.
Woo, N.S., Lu, J., England, R., McClellan, R., Dufour, S., Mount, D.B., Deutch, A.Y., Lovinger, D.M., Delpire, E., 2002. Hyper-excitability and epilepsy associated with disruption of mouse neuronal-specific K-CL cotransporter gene. Hippocampus 12, 258–268.
Xu, J.C., Lytle, C., Zhu, T.T., Payne, J.A., Benz Jr., E., Forbush 3rd, B., 1994. Molecular cloning and functional expression of the bumetanide-sensitive Na-K-Cl cotransporter. Proc. Natl. Acad. Sci. U.S.A. 91, 2201–2205.
Yamada, R., Okuda, H., Kuba, H., Nishino, E., Ishii, T.M., Ohmori, H., 2013. The cooperation of sustained and phasic inhibitions increases the contrast of ITD-tuning in low-frequency neurons of the chick nucleus laminaris. J. Neurosci. 33, 3927–3938.
Yang, L., Monsivais, P., Rubel, E.W., 1999. The superior olivary nucleus and its influence on nucleus laminaris: a source of inhibitory feedback for coincidence detection in the avian auditory brainstem. J. Neurosci. 19, 2313–2325.
Zafra, F., Castrén, E., Thoenen, H., Lindholm, D., 1991. Interplay between glutamate and gamma-aminobutyric acid transmitter systems in the physiological regulation of brain-derived neurotrophic factor and nerve growth factor synthesis in hippocampal neurons. Proc. Natl. Acad. Sci. U.S.A. 88, 10037–10041.